Available online at www.sciencedirect.com
SCIENCE DIRECT®
Journal of Organometallic Chemistry 677 (2003) 101–117
Journal of Organometallic Chemistry
www.elsevier.com/locate/jorganchem

Iron carbonyl complexes of heterocyclic α-diimines: systematic synthesis, crystal structures of $[Fe(CO)_3(L)]$ and $[Fe_2(CO)_7(L)]$ (L = 2,2′-bipyridine and 1,10-phenantroline), and their AIM analysis☆

Meritxell DelaVarga [a], Ramon Costa [a,*], Roser Reina *, Alberto Núñez [b], Miguel Ángel Maestro [b], José Mahía [b]

[a] Departament de Química Inorgànica, Universitat de Barcelona, Martí i Franquès 1-11, E-08028 Barcelona, Spain
[b] Servicios Xerais de Apoio á Investigación, Universidade da Coruña Edificio Anexo Facultade de Ciencias, E-15071 A Coruña, Spain

Received 11 February 2003; received in revised form 29 April 2003; accepted 29 April 2003

Abstract

Heterocyclic α-diimines {2,2′-bipyridine (bpy), 4,4′-dimethyl-2,2′-bipyridine (4,4′-Me_2bpy), 1,10-phenantroline (phen), 4,7-dimethyl-1,10-phenantroline (4,7-Me_2phen) and 2,9-dimethyl-1,10-phenantroline (2,9-Me_2phen)} react, in a wide range of conditions, with iron clusters of nuclearity one, two or three. Two kinds of compounds, $[Fe(CO)_3(\alpha\text{-diimine})]$ (type **1**) and $[Fe_2(CO)_7(\alpha\text{-diimine})]$ (type **2**), are afforded in all cases. We propose a reaction mechanism to explain this behaviour. The crystal structures of compounds $[Fe(CO)_3(bpy)]$ (**1a**), $[Fe(CO)_3(phen)]$ (**1b**), $[Fe_2(CO)_7(bpy)]$ (**2a**) and $[Fe_2(CO)_7(phen)]$ (**2b**) at 173 K were determined by single-crystal X-ray diffraction methods. In contrast, reaction of the pentanuclear iron cluster $[Fe_5C(CO)_{15}]$ with bpy led to the tetranuclear salt $[Fe(bpy)_3][(\mu\text{-H})Fe_4C(CO)_{12}]_2$ (**3**). The electronic structures of the mono- and di-iron derivatives with bpy and phen were analysed using the atoms in molecules (AIM) theory. Their comparative study seems to rule out the existence of Fe–Fe bond in the dinuclear complexes.

Keywords: Iron; α-Diimines; Carbonyl; Complexes; AIM

1. Introduction

During the last 30 years, a great variety of transition-metal carbonyl complexes containing α-diimines have been reported [1]. Because of their spectroscopic and photochemical properties, they have potential applications in synthetic and catalytic processes. These versatile ligands can be classified in three groups depending on how many of the imine units belong to aromatic rings, as shown in Scheme 1.

Type A compounds such as 2,2′-bipyridine and 1,10-phenantroline are used as chelating ligands. Their ruthenium carbonyl derivatives are widely studied, given their high thermodynamic stability and ease of crystallization. More than 80 complexes, with nuclearity ranging from 1 to 5, have been structurally characterized [1–4]. This contrasts with the paucity of osmium and iron carbonyls containing coordinated heterocyclic α-diimines. For the former, only triangular $[Os_3(CO)_{12}]$ and tetrahedral $[Os_4(\mu\text{-H})_4(CO)_{12}]$ monosubstituted derivatives are known [5], while iron forms only mono- and dimetallic compounds.

The first complex of iron carbonyls with nitrogen ligands was $[Fe(CO)_4NH_3]$, described in 1962 [6], while the first structural characterization was reported on a cyclometallate in 1966 [7]. Several structures of di-iron

☆ Presented in part at the 34th International Conference on Coordination Chemistry held in Edinburgh (Great Britain), in July 2000, abstract P0337; and in the XIX Reunión del Grupo Especializado de Química Organometálica, held in Valladolid (Spain), in July 2000, abstract PC44.

* Corresponding authors. Tel.: +34-934021271; fax: +34-934907725.
E-mail address: ramon.costa@qi.ub.es (R. Costa).

0022-328X/03/$ - see front matter © 2003 Elsevier Science B.V. All rights reserved.
doi:10.1016/S0022-328X(03)00381-4

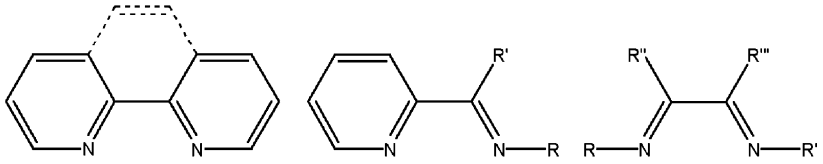

Scheme 1.

compounds with bridging N-donors were published and the first chelate complex was characterized in 1968: the iron pentacarbonyl disubstitution complex of the 1,4-dimethyltetraaza-1,3-diene ligand [8], which is type C. In 1974, Cotton and Troup [9] reported the characterization of iron carbonyl complexes with N-containing heterocyclic ligands: in addition to the monodentate ligand $[Fe(CO)_4L]$ derivatives (L = pyridine or imidazole) they obtained $[Fe_2(CO)_7(2,2'\text{-bipyridine})]$ [10]. Although the reaction yield was limited to some monocrystals, the latter compound was the first example of an α-diimine complex of iron carbonyl to be structurally characterized. To our knowledge, no more than 25 iron complexes of this kind are known by their X-ray structures [10–28]. Of these, only two [10,28] are pure type A carbonyldiimine complexes with no additional ligands. Although in 1983 Frühauf [29] published the synthesis and characterization of $[Fe_2(CO)_7(L)]$ by photolysis of $[Fe(CO)_5]$ in the presence of the corresponding ligand and that of $[Fe(CO)_3(L)]$, (L = 2,2′-bipyridine, 1,10-phenantroline) departing from the benzylideneacetone complex [30], no structures were reported for the new 1,10-phenantroline complexes.

In this contribution, we examine the reactivity of heterocyclic α-diimines with iron carbonyl clusters of various nuclearities in order to design a general synthetic methodology for all such complexes and characterize the resulting compounds. We studied the reactions of $[Fe(CO)_5]$, $[Fe_2(CO)_9]$, $[Fe_3(CO)_{12}]$ and $[Fe_5C(CO)_{15}]$ with the α-diimines 2,2′-bipyridine (bpy, **a**), 1,10-phenantroline (phen, **b**), 4,4′-dimethyl-2,2′-bipyridine (4,4′-Me_2bpy, **c**), 4,7-dimethyl-1,10-phenantroline (4,7-Me_2-phen, **d**) and 2,9-dimethyl-1,10-phenantroline (2,9-Me_2-phen, **e**) in a range of conditions. Fragmentation processes were observed for nuclearities of 3 and higher. For $[Fe_3(CO)_{12}]$, they led to the formation of mono- and di-iron derivatives, which were characterized. For $[Fe(CO)_5]$ and $[Fe_2(CO)_9]$, the same final products were found in similar proportions, and so we propose a reaction mechanism in order to explain this behaviour.

The crystal structures of $[Fe(CO)_3(bpy)]$, $[Fe(CO)_3(phen)]$, $[Fe_2(CO)_7(bpy)]$ and $[Fe_2(CO)_7(phen)]$ at 173 K are reported. While this paper was in preparation, Calderazzo et al. [28] described the formation and crystal characterization of $[Fe(CO)_3(bpy)]$ from $FeR_2(bpy)_2$ (R = Me, Et) in the presence of CO by reductive elimination of dialkylketones, and so the structures of the 2,2′-bipyridine derivatives have been examined in greater depth and new insights have been reported.

The di-iron complexes were analysed using the atoms in molecules (AIM) theory [31], and their electronic structure was compared to that of di-iron nonacarbonyl.

2. Results and discussion

2.1. Reactivity of the α-diimines with iron carbonyls

2.1.1. Reactions with $[Fe_3(CO)_{12}]$

In an attempt to obtain tri-iron derivatives, we assayed the reaction of the tri-iron dodecacarbonyl with α-diimines in a range of experimental conditions. Direct reaction of $[Fe_3(CO)_{12}]$ with bpy (**a**) in THF was slow even at r.t., whereas no reaction was observed for phen (**b**). Trimethylamine oxide (TMNO) was thus used as initiator at a range of molar relations and temperatures (from −78 °C to r.t.). In all cases, reaction was observed immediately. IR spectroscopy showed a shift of the ν(CO) cluster bands to lower frequencies, as expected for the replacement of two carbonyl groups by one α-diimine ligand. The assays were stopped once the spectra were constant.

TLC analysis of the solids revealed two main derivatives for each α-diimine. These fractions were separated by column chromatography and layered with toluene/hexane at ca. −30 °C. Although ^{1}H- and ^{13}C-NMR spectroscopy of the remaining products showed ligand coordination (see Table 1), elemental analyses of the fractions did not agree with any expected product (see Section 3). Further recrystallization yielded single crystals of the two reaction products obtained from each α-diimine. X-ray analyses identified the reaction products as mixtures of mononuclear $[Fe(CO)_3(\alpha\text{-diimine})]$ derivatives (type **1** products) and di-iron $[Fe_2(CO)_7(\alpha\text{-diimine})]$ complexes (type **2** products). We had previously ruled out their presence in the reaction solution as our experimental spectroscopic data did not agree with that reported by Frühauf [29,32]. The recently published IR spectrum of **1a** in Nujol [28] agrees rather well with our observations.

Table 1
^{1}H- and ^{13}C{^{1}H}-NMR spectral data and assignment [a] for complexes **1a**·0.5$C_{10}H_8N_2$, **1b**–**1e** and **2a**–**2e** (see numbering in Scheme 2)

Complex	^{1}H-NMR						^{13}C{^{1}H}-NMR								
	H_2	H_3	H_4	H_5	H_6	CH_3	C_2	C_3	C_4	C_5	C_6	C_{11}	C_{12}	CH_3
1a [b]		6.99	6.62	6.18	9.07		150.2	121.5	129.3	120.9	153.2			
1b	9.26 d, $J = 5.5$	6.57 t, $J = 6.5$	6.90 d [b]	7.12 s			152.4	121.5	126.3	128.8		130.6	142.9	
1c [b]		6.98		6.09	9.02	1.74	150.2	121.7	141.4	123.0	152.8			20.1
1d [c,b]	9.25	7.31		8.48		2.02	151.4	125.3	150.5	124.2		128.2	155.1	18.9
1e [d]		6.69 d $J = 8.2$	7.24 d, $J = 8.2$	7.06 s		3.06 s								
2a [b]		6.94 d	6.65 t	6.15 t	8.67 d		153.6	122.2	135.5	124.0	151.6			
2b	8.92 d, $J = 4.5$	6.40 m	7.09 d, $J = 8.0$	6.95 s			151.8	123.6	134.6	126.7		130.6	145.5	
2c		6.87 s		6.01 d, $J = 5.0$	8.56 d, $J = 5.0$	1.60 s	153.1	122.8	147.2	125.6	150.8			21.2
2d [c]	9.06 d, $J = 5.5$	7.97 d, $J = 5.5$		8.43 s		3.00 s	153.0	127.2	148.6	125.4		130.3	154.6	19.3
2e [d]		6.73 d $J = 8.0$	7.38 d, $J = 8.0$	7.10 s		3.52 s								

[a] Assignments were performed with the help of both free ligand and complex heterocorrelation experiments.
[b] Band broadening does not allow the ^{1}H–^{1}H coupling constant calculation.
[c] Spectra measured in acetone-d_6.
[d] ^{13}C data were not recorded due to sample decomposition during acquisition.

The best reaction yields were found at low temperature (Bruce et al. [33] suggest working below −30 °C in order to avoid the tri-iron cluster fragmentation) and excesses of TMNO (1:2,1) and diimine (1:1,5) over carbonyl. These factors were also favoured the synthesis of other iron derivatives [34]. Nevertheless, even in the optimal conditions, the weight of final solid product was less than 1/10 that of the starting cluster for both **a** and **b** α-diimines, thus indicating severe cleavage and decomposition of the departing carbonyl.

We subsequently replaced the activator from TMNO by the less aggressive Ph_2CO^- activator in order to preserve the cluster integrity. A solution of $[Fe_3(CO)_{12}]$ in THF was then treated with phen (**b**) and benzophenone/Na in tetrahydrofuran (THF) at −30 °C. Two products were detected, separated by column chromatography and identified as the mono- and di-iron derivative, respectively. In this case, the reaction afforded 60% yields of compound **2b** and traces of compound **1b**. Similar results were obtained by using the dimethyl derivative 4,7-Me_2phen (**d**), but for 2,9-Me_2phen (**e**) the majority product was **1e**. Steric hindrance from the methyl substituents near the donor atoms in the latter ligand probably destabilizes the di-iron derivative. ^{1}H- and ^{13}C-NMR data of all the products are summarized in Table 1.

Finally, we used toluene as solvent instead of THF in order to minimize the $[Fe_3(CO)_{12}]$ cleavage (IR experiments showed that the integrity of the triangular cluster is better conserved in toluene than in THF solutions). The reaction was slow even with the use of initiators at r.t., and most of the starting cluster was recovered. Although the resulting products were the same as with THF, their yield was much lower.

At this stage, it was clear that the synthetic methods would need to be improved in order to obtain sufficient amounts of complexes of types **1** and **2** for spectroscopic characterization.

2.1.2. Reactions with $[Fe_2(CO)_9]$

We re-examined the reactivity of di-iron nonacarbonyl with the **a**–**e** α-diimines in our experimental conditions. We reacted $[Fe_2(CO)_9]$ with α-diimine in THF at −78 °C in an inert atmosphere in the presence of TMNO as initiator. Two products were separated by column chromatography. They were both a mixture of mono- and di-iron derivatives, the yields of which were

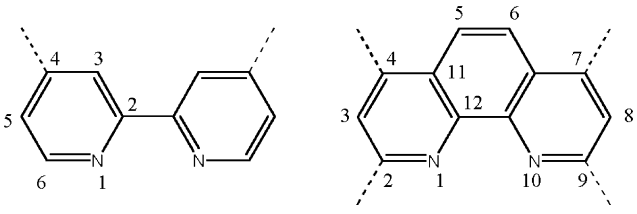

Scheme 2.

approximately 20% for **1a**–**1d** and 65% for **2a**–**2d**. 2,9-Me_2phen (**e**), afforded **1e** in 90% yield and **2e** in 7% yield (a similar ratio was obtained by Ackermann et al. [35] in the reaction of $[Fe_2(CO)_9]$ with 2-(phenylazo)pyridine ligands in THF, whereas only di-iron derivative formation was reported by Cotton and Troup [10]). For phen and its derivatives, we observed that the reaction solution is initially blue (which indicates the presence of mono-iron complexes) and then turns slowly to violet (formation of di-iron complexes) except for 2,9-Me_2-phen, which remains blue as **1e** is the majority product. Recent papers also describe the formation of mono- and dinuclear iron carbonyl derivatives when di-iron nonacarbonyl is reacted with ligands containing a nitrogen or a sulphur atom in the β-position of ketone groups [36]. An explanation of these findings is proposed below.

2.1.3. Reactions with $[Fe(CO)_5]$ and $[Fe(CO)_3(bda)]$

In order to obtain type **1** compounds, we react iron pentacarbonyl in an inert atmosphere with 2,2′-bipyridine (**a**) following the same procedure as described for the reaction of di-iron nonacarbonyl. Unexpectedly, the majority reaction product was **2a** (64% yield vs. 18% for **1a**).

With the aim of obtaining majority type **1** products, we followed the synthetic methodology reported for some dienes [37,38] and 1,4-diaza-1,3-butadiene [34,39] derivatives, which departs from benzylideneacetone (bda) derivatives. The new set of reactions was performed by the treatment of $[Fe(CO)_3(bda)]$ with the α-diimines **a**–**d** in toluene at room temperature, which afforded blue solutions. The reactions were monitored by IR spectroscopy and they were considered to be finished when the 2065 cm^{-1} band of the starting complex disappeared. The desired derivatives were purified by column chromatography and recrystallized by slow layer diffusion. The yield of the reactions was around 50% of exclusively type **1** products.

2.1.4. Reactivity of $[Fe_5C(CO)_{15}]$ with 2,2′-bpy

Although $[Fe_3(CO)_{12}]$ cleaves in the presence of α-diimine ligands leading to di-iron and mono-iron derivatives, the tetra [3] and pentaruthenium [4] analogues react with 2,2′-bipyridine (**a**) affording high nuclearity derivatives. In order to assess whether the neutral and quite stable iron carbonyl $[Fe_5C(CO)_{15}]$ renders similar species, we examined its reactivity with 2,2′-bipyridine. We assayed the reaction in THF solution at −78 °C with and without initiators (TMNO and Na/benzophenone). ν(CO) shifted to lower frequencies and the work up of the reaction afforded brown crystals. The X-ray crystal structure revealed that the product was the complex salt $[Fe(bpy)_3][(\mu\text{-}H)Fe_4C(CO)_{12}]_2$ (**3**). Although both ions have been described separately in the literature [36,40], the crystallographic data of this new complex are deposited as supplementary material.

2.2. Mechanism

Di-iron nonacarbonyl has been widely used as the starting product in the preparation of substituted iron carbonyls, but its low solubility in most solvents requires long reaction times that can favour decomposition of some of the reactants. Some authors [9,10] have examined the $[Fe_2(CO)_9]$ dissolution process in THF, as it reacts with the solvent leading to reactive intermediates that shorten reaction times and optimize yields. We next provide some insights on this subject.

IR spectroscopy revealed four features of the reactions of iron carbonyls and α-diimines in THF: (a) in all experiments, the first new bands to appear were those due to the mononuclear tricarbonyl iron complexes (type **1**), consistent with the initial blue coloration observed in the assays with phen derivatives, with further intensification of the bands corresponding to type **2** derivatives; (b) in addition to the bands belonging to type **1** and **2** derivatives, two additional unidentified bands at 1969 and 1930 cm^{-1} appeared; (c) the 1969 cm^{-1} band was also detected when THF solutions of $[Fe_3(CO)_{12}]$ or $[Fe_2(CO)_9]$ stood for several hours; (d) assays with no activator led to the same final complexes, although in low yields.

We can conclude that when starting iron clusters are dissolved in THF they fragment even in the absence of an activator, yielding intermediate iron carbonyls with a vacant position, which can be temporarily occupied by THF (stretching at 1969 cm^{-1} [9]). If Me_3NO is used to create the vacancy, the position is occupied by the trimethylamine formed in the reduction of the N-oxide, showing a characteristic band at 1930 cm^{-1}. Later, these intermediate species are displaced by the chelating diimine, yielding $[Fe(CO)_3(\alpha\text{-diimine})]$ complexes. The mono-iron derivatives progress to the di-iron compounds $[Fe_2(CO)_7(\alpha\text{-diimine})]$ by reaction with one more intermediate fragment until the equilibrium conditions are reached. The mechanism proposed is summarized in Scheme 3.

This mechanism would explain why both type **1** and **2** products are always formed in THF, despite the nuclearity of the departing iron cluster, and independent of the molar ratio of α-diimine or the presence of initiators. It also explains why the use of initiators, especially TMNO, speeds the reaction, diminishing the decomposition of the products and thus improving yields.

2.3. Crystal structures

2.3.1. $[Fe(CO)_3(bpy)]\cdot 0.5bpy$ (**1a**)

The crystal structure of compound **1a** at room temperature has recently been described by Calderazzo et al. [28]. Our results at 173 K have showed no

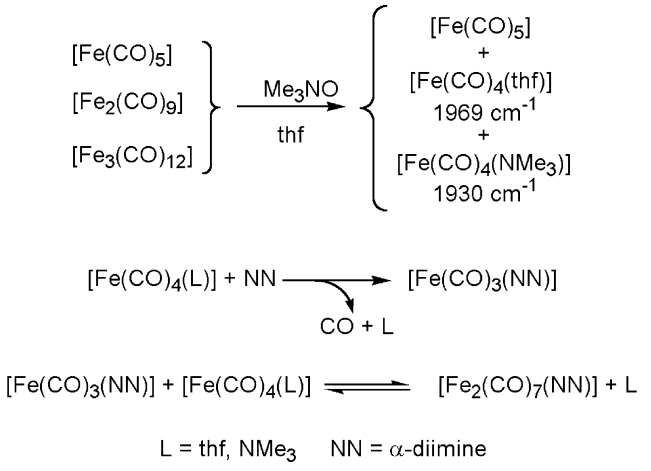

Scheme 3.

significant differences, but a short description is offered and some features that may have been overlooked in previous studies are mentioned. The molecular structure and atom labelling are shown in Fig. 1. Selected bond lengths and angles are listed in Table 2.

In the metallic complex, the central iron(0) atom is bound to three CO molecules and to one bpy ligand. The latter acts as a bidentate ligand, thus yielding a five-member chelate. The study of the pentacoordination around the metal points to a trigonal bipyramidal (TBPY) geometry, with a small distortion to square-pyramidal (SPY). Homes' [41] analysis of the dihedral angles gives 84% Berry pseudo-rotation from SPY to TBPY when fixing C(3) as the pivot atom, whereas the

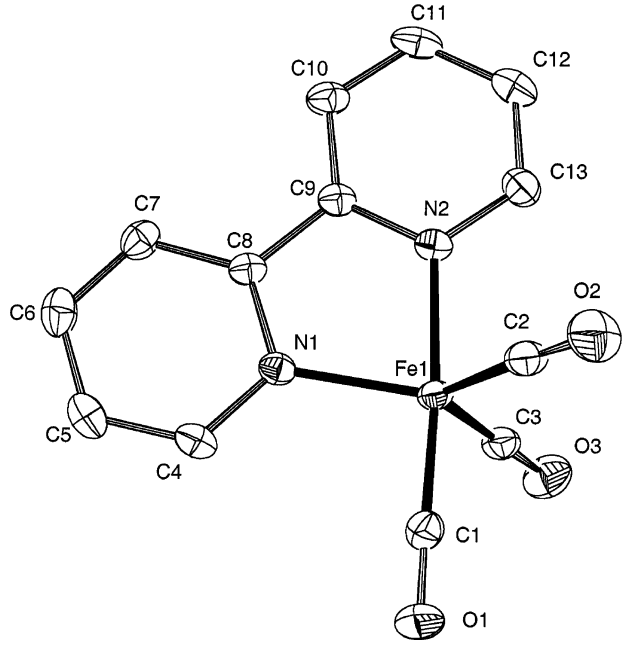

Fig. 1. ORTEP view of the molecular structure of the organometallic moiety **1a** of $[Fe(CO)_3(bpy)]\cdot 0.5C_{10}H_8N_2$. Thermal ellipsoids are drawn at 50% probability level. H atoms have been omitted for clarity.

Table 2
Selected bond lengths (Å) and angles (°) for complexes **1a**·$0.5C_{10}H_8N_2$, **1b**, **2a** and **2b** (standard deviation parameters are given in parentheses)

	1a·$0.5C_{10}H_8N_2$	**1b**	**2a**	**2b**
Bond lengths				
Fe(1)–Fe(2)			2.6115(4)	2.5950(4)
Fe(1)–N(1)	1.9926(14)	1.9853(19)	2.0363(15)	2.0539(15)
Fe(1)–N(2)	1.9766(14)	2.0044(19)	2.0259(15)	2.0486(16)
Fe(1)–C(1)	1.7610(19)	1.781(2)	1.777(2)	1.787(2)
Fe(1)–C(2)	1.785(2)	1.764(2)	1.785(2)	1.792(2)
Fe(1)–C(3)	1.776(2)	1.763(2)	2.404(2)	2.330(2)
Fe(1)–C(4)			1.8908(19)	1.902(2)
Fe(2)–C(3)			1.8236(19)	1.840(2)
Fe(2)–C(4)			2.0443(19)	2.050(2)
Fe(2)–C(5)			1.816(2)	1.824(2)
Fe(2)–C(6)			1.826(2)	1.825(2)
Fe(2)–C(7)			1.792(2)	1.795(2)
O(1)–C(1)	1.156(2)	1.150(3)	1.152(2)	1.146(3)
O(2)–C(2)	1.152(2)	1.156(3)	1.144(3)	1.147(3)
O(3)–C(3)	1.158(3)	1.149(3)	1.157(2)	1.162(3)
O(4)–C(4)			1.180(2)	1.178(2)
O(5)–C(5)			1.139(3)	1.144(3)
O(6)–C(6)			1.137(3)	1.143(3)
O(7)–C(7)			1.141(3)	1.150(3)
Bond angles				
N(1)–Fe(1)–N(2)	79.74(6)	80.89(7)	79.59(6)	80.55(6)
N(1)–Fe(1)–C(1)	95.38(7)	92.47(9)	93.11(7)	93.30(8)
N(1)–Fe(1)–C(2)	125.98(8)	93.06(9)	107.51(7)	102.78(8)
N(1)–Fe(1)–C(3)	119.46(7)	175.08(9)	80.53(6)	82.68(7)
N(1)–Fe(1)–C(4)			159.25(8)	163.18(9)
N(2)–Fe(1)–C(1)	174.65(8)	118.12(10)	172.64(8)	173.16(8)
N(2)–Fe(1)–C(2)	91.32(7)	130.33(10)	91.58(7)	94.52(8)
N(2)–Fe(1)–C(3)	93.71(7)	94.86(9)	78.64(6)	80.53(7)
N(2)–Fe(1)–C(4)			92.93(7)	90.86(8)
C(1)–Fe(1)–C(2)	89.80(8)	111.34(11)	91.48(9)	89.73(10)
C(1)–Fe(1)–C(3)	90.61(9)	91.71(10)	99.41(8)	95.81(9)
C(1)–Fe(1)–C(4)			93.66(8)	94.34(10)
C(2)–Fe(1)–C(3)	114.19(9)	87.81(10)	166.19(8)	172.02(9)
C(2)–Fe(1)–C(4)			91.90(9)	92.22(10)
C(3)–Fe(1)–C(4)			79.03(8)	81.66(9)
C(3)–Fe(2)–C(4)			90.91(8)	91.32(8)
C(3)–Fe(2)–C(5)			90.87(9)	91.93(9)
C(3)–Fe(2)–C(6)			166.97(9)	166.64(10)
C(3)–Fe(2)–C(7)			94.78(9)	92.70(10)
C(4)–Fe(2)–C(5)			157.79(9)	155.41(10)
C(4)–Fe(2)–C(6)			82.40(8)	80.35(9)
C(4)–Fe(2)–C(7)			97.81(9)	97.30(10)
C(5)–Fe(2)–C(6)			91.18(9)	91.45(9)
C(5)–Fe(2)–C(7)			104.09(9)	106.88(11)
C(6)–Fe(2)–C(7)			97.19(9)	98.67(10)
Fe(1)–C(1)–O(1)	178.68(18)	172.7(2)	170.04(18)	167.4(2)
Fe(1)–C(2)–O(2)	175.15(18)	172.2(2)	174.18(18)	173.29(19)
Fe(1)–C(3)–Fe(2)			74.90(7)	75.95(8)
Fe(1)–C(3)–O(3)	175.25(16)	177.7(2)	122.88(14)	124.75(16)
Fe(2)–C(3)–O(3)			162.20(18)	159.27(19)
Fe(1)–C(4)–Fe(2)			83.06(7)	82.00(8)
Fe(1)–C(4)–O(4)			142.46(16)	142.79(17)
Fe(2)–C(4)–O(4)			134.48(15)	135.21(16)
Fe(2)–C(5)–O(5)			176.9(2)	177.27(19)
Fe(2)–C(6)–O(6)			177.5(2)	176.94(19)
Fe(2)–C(7)–O(7)			178.68(19)	179.2(2)

Addison's τ parameter [42] indicates an 81% TBPY character. The bpy ligand occupies one equatorial [N(1)] and one axial [N(2)] position, which minimizes the strain of the chelate ring. The C(1) atom occupies the remaining axial position with a C(1)–Fe(1)–N(2) angle of 174.66(7)°.

The analysis of the crystal packing suggests significant intermolecular π-stacking interactions between the heterocyclic rings of the aromatic ligands. The metallic complexes are arranged in two alternating opposite orientations and form an stack along the x-axis as in a zip fastener. The bpy ligands of the metallic moieties lie in nearly parallel orientation in the inner part, in such a way that every bpy ligand overlaps with its upper and lower neighbours. The metallic $Fe(CO)_3$ fragments lie alternately on each side of the exterior (see Fig. 2).

These interactions have been analysed by means of four parameters (see Scheme 4): (a) the dihedral angle α between the main planes of the interacting rings; for effective interactions, it should be close to zero; (b) the distance D between their centroids; (c) the normal distances from the mean plane containing one ring to the centroid of the other, N_{AB} and N_{BA}; they are coincident for parallel rings; (d) the displacement angles β and γ between the vector D and the normal vectors N_{AB} and N_{BA} (they are coincident for parallel rings). The lower the values for the four parameters, the more the rings overlap, and the more efficient the interaction.

The parameters of the interactions between the rings for compound **1a** are summarized in Table 3. For the metallic stack, there are two distinct separations between the interacting rings. The ligand pairs with shortest normal distances (3.41 Å mean) have the greatest separation between centroids and the highest displacement angles. The couples with longest normal vectors (3.50 Å mean) overlap better as both the centroid separation and the displacement angles are smaller.

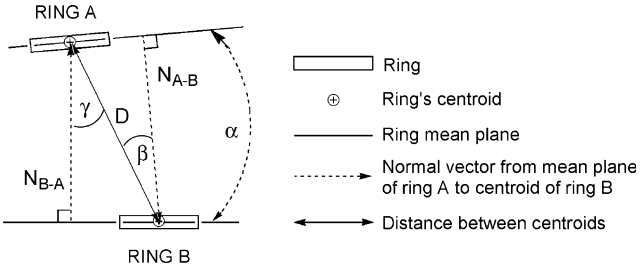

Scheme 4.

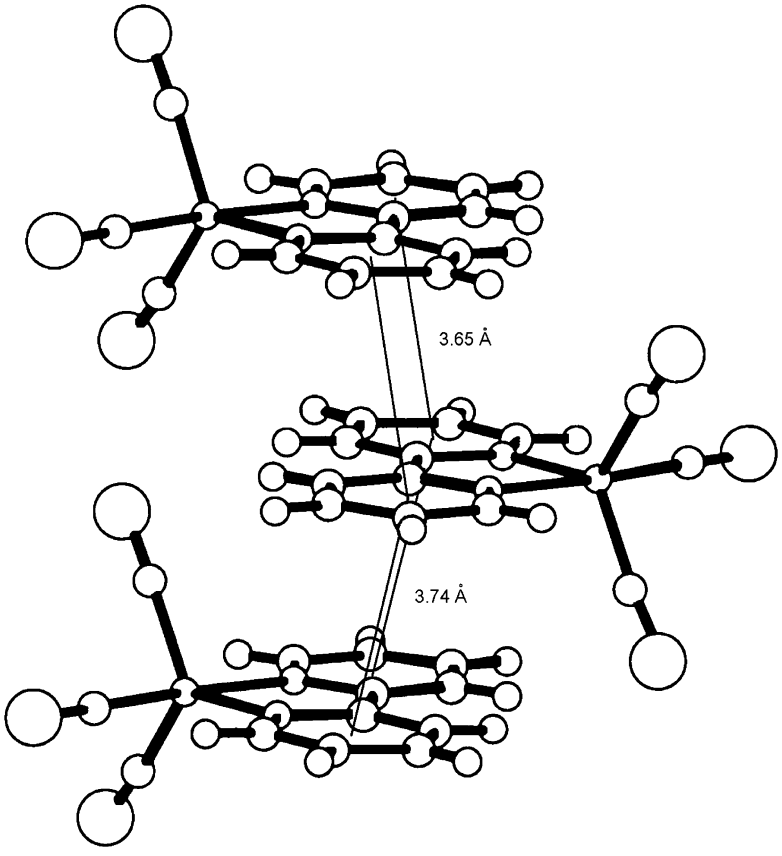

Fig. 2. π-Stacking interactions in the moiety $[Fe(CO)_3(bpy)]$ (**1a**).

The free bpy molecules crystallize in trans-planar conformation and also stack along the x-axis. Their rings are parallel and form an angle of 28.6° with the stacking direction. This sharp angle together with the unfavourable distance between centroids and deviation angles (smallest values of 4.08 Å and 32.2°, respectively) prevent efficient π-overlap between the rings.

Both kinds of stacks lie intercalated in a chessboard manner (see Fig. 3). This arrangement allows weak H-bond interactions [43] between the stacks. Furthermore the H(13) atom of the chelating 2,2′-bipyridines interacts with the π-system of the free bpy aromatic rings. The crystallographic parameters of these feeble interactions are listed in Table 3. A weak C(4)–H(4)···N(3) hydrogen bond binds the coordinated and the free bpy molecules. They may contribute to the stabilization of the solid frame, revealing the role of the free bpy molecules in the formation of crystals of **1a**.

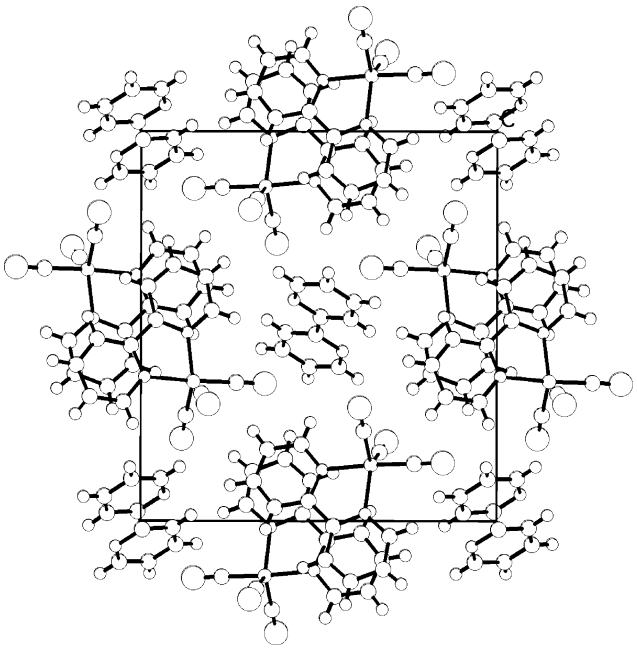

Fig. 3. View of the crystal cell of $[Fe(CO)_3(bpy)]\cdot 0.5C_{10}H_8N_2$ along the x-axis emphasizing the alternate stacks of the **1a** and $C_{10}H_8N_2$ moieties and how they are interconnected.

2.3.2. *[Fe(CO)$_3$(phen)] (**1b**)*

The crystal structure of compound **1b** consists of a packing of $[Fe(CO)_3(phen)]$ molecular complexes (Fig. 4). Selected bond lengths and angles are listed in Table 2.

The neutral iron atom is bonded to three carbonyl moieties and to a 1,10-phenantroline ligand, which acts as a chelate, giving a pentacoordinated environment similar to that described for **1a**. The geometry is still mainly TBPY, with C(1), C(2) and N(2) atoms placed in the equatorial positions and C(3) and N(1) in the axial. Nevertheless, the distortion to SPY is greater than in **1a**: the TBPY character is 77 and 75% according to Homes' (using C(1) as pivot atom) and Addison's methods, respectively.

The crystal packing of **1b** shows π-stacking interactions between the aromatic ligands along the y-axis, favoured by the alternating opposite arrangement of the molecules (see Fig. 5). There are two kinds of aromatic overlap whose crystallographic parameters are listed in Table 3. The most efficient interaction takes place between the parallel heterocyclic rings containing N(1) of two adjacent complexes, with a short D separation of 3.57 Å and a small deviation angle of 10.3°. On the alternate interaction, there is a double π contact: the heterocyclic rings containing N(1) of each molecule overlap with the benzene ring of its neighbour. In this case, the overlaps seem weaker than before: rings are not parallel ($\alpha = 1.3$), whereas the centroid separation (3.64 Å) and the displacement angles (20.6 and 21.6°) are greater. A weak hydrogen interaction between C(9)–H(9)···O(2) atoms strengthens the stack ordering. The additional C(4)–H(4)···O(1) interaction may contribute to the cohesion between adjacent stacks.

2.3.3. *[Fe$_2$(CO)$_7$(bpy)] (**2a**)*

As for compound **1a**, the crystal structure of compound **2a** at room temperature was early described by Cotton and Troup [10] in 1974. Our results at 173 K are not significantly different, but some unnoticed features are reported. The molecular structure and atom labelling is shown in Fig. 6. Selected bond lengths and angles are listed in Table 2.

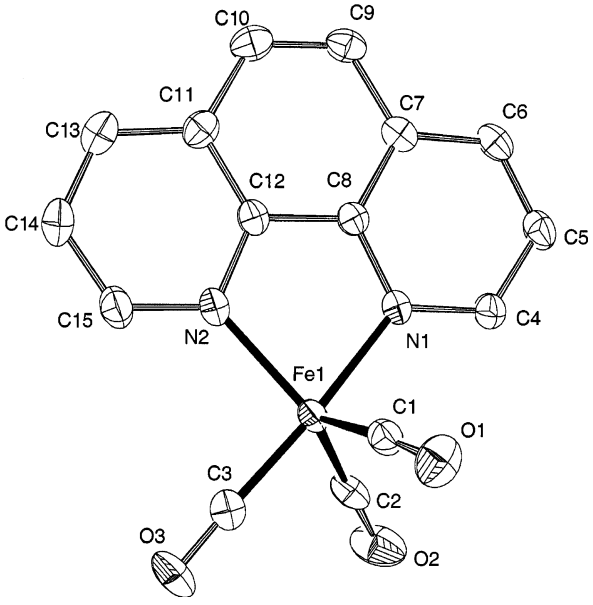

Fig. 4. ORTEP view of the molecular structure of $[Fe(CO)_3(phen)]$ (**1b**). Thermal ellipsoids are drawn at 50% probability level. H atoms have been omitted for clarity.

Table 3
Summary of the geometric parameters of the ring–ring π-stacking interactions for compounds **1a**·0.5$C_{10}H_8N_2$, **1b**, **2a** and **2b**

Compound, ring's centroids	**1a**·0.5$C_{10}H_8N_2$ [c], Cg(2 [a])–Cg(3 [b])	**1a**·0.5$C_{10}H_8N_2$ [e], Cg(2 [a])–Cg(3 [d])	**1a**·0.5$C_{10}H_8N_2$, Cg(4 [a])–Cg(4 [f])	**1b**, Cg(2 [a])–Cg(2 [g])	**1b** [i], Cg(2 [a])–Cg(4 [h])	**2a** [k], Cg(1 [a])–Cg(2 [j])	**2b** [m], Cg(1 [a])–Cg(3 [l])	**2b**, Cg(3 [a])–Cg(3 [n])
α (°)	1.6	1.6	0.0	0.0	1.3	5.0	2.3	0.0
D (Å)	3.65	3.74	4.08	3.57	3.64	3.62	3.64	3.62
β (°)	15.7	24.3	32.2	10.3	20.6	20.2	20.6	26.1
γ (°)	17.1	24.1	32.2	10.3	21.6	24.8	22.9	26.1
N_{A-B} (Å)	3.49	3.42	3.45	3.52	3.39	3.29	3.36	3.25
N_{B-A} (Å)	3.51	3.41	3.45	3.52	3.41	3.40	3.41	3.25

Each ring's centroid Cg(i) is numbered accordingly to the crystallographic label of the nitrogen atom that contains. When $\alpha \neq 0$, it exists the complementary interaction for which the β and γ, and the N_{A-B} and N_{B-A} parameters must be exchanged.

[a] x, y, z.
[b] $2-x, 1-y, -z$.
[c] Also Cg(3[a])–Cg(2[b]).
[d] $1-x, 1-y, -z$.
[e] Also Cg(3[a])–Cg(2[d]).
[f] $2-x, -y, -z$.
[g] $2-x, 1-y, -z$.
[h] $2-x, 2-y, -z$.
[i] Also Cg(4[a])–Cg(2[h]).
[j] $-x, 1-y, 1-z$.
[k] Also Cg(2[a])–Cg(1[j]).
[l] $-x, 1-y, 1-z$.
[m] Also Cg(3[a])–Cg(1[l]).
[n] $1-x, 1-y, 1-z$.

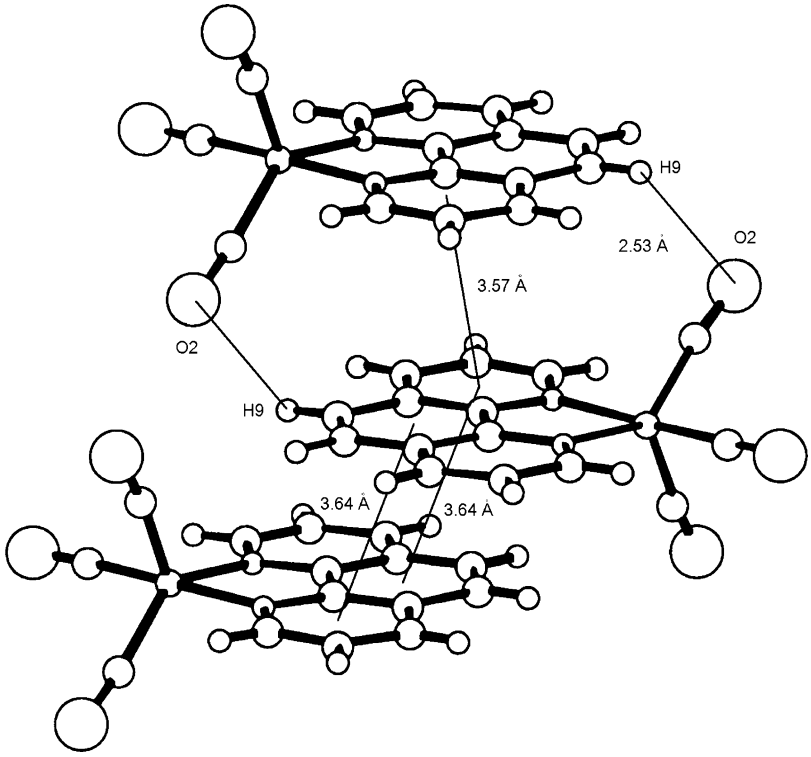

Fig. 5. π-Stacking interactions in $[Fe(CO)_3(phen)]$ (**1b**).

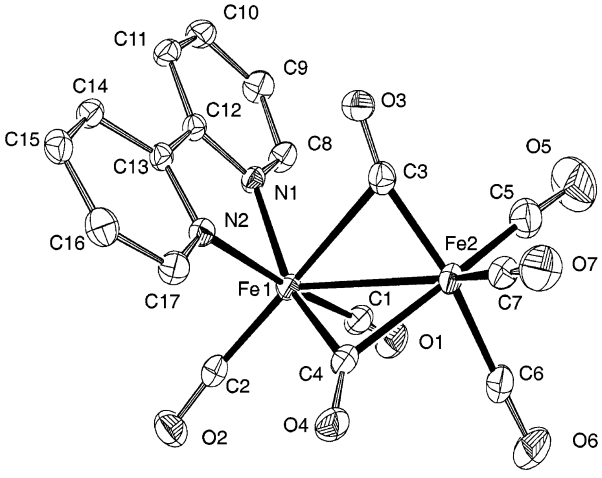

Fig. 6. ORTEP view of the molecular structure of $[Fe_2(CO)_7(bpy)]$ (**2a**). Thermal ellipsoids are drawn at 50% probability level. H atoms have been omitted for clarity.

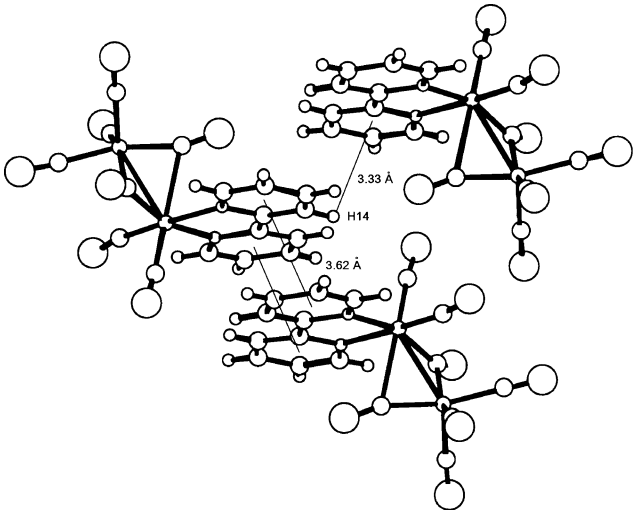

Fig. 7. π-Stacking interactions in $[Fe_2(CO)_7(bpy)]$ (**2a**).

The molecule consists of a dinuclear iron(0) cluster. The Fe(1) atom is surrounded by six donor atoms: N(1) and N(2) from the chelating bpy ligand, and C(1), C(2), C(3) and C(4) belonging to carbonyl ligands. The geometry around this metal can be viewed as a distorted octahedron: the *trans* angles vary from 159.2 to 172.6°, and the *cis* angles range from 78.6 to 107.5° with a mean value of 90(9)°. The Fe(2) centre is directly bound to five carbonyl ligands, from CO(3) to CO(7). The carbon atoms C(3), C(4), C(5) and C(6) are 0.09 Å inside their least-squares plane, and the Fe(2) is 0.28 Å displaced from it towards the CO(7) ligand. This suggests SPY geometry, which is confirmed by the low TBPY character calculated: 15% according to Addison parameter and 13% according to Homes using the apical donor atom C(7) as pivot.

The carbonyls CO(3) and CO(4) act as μ^2-bridging ligands. The geometrical classifications of Colton and McCormick [44] and Cotton and Troup [45] coincide in considering the CO(4) ligand as an asymmetric bridging carbonyl and the CO(3) as a semibridging one. The spatial arrangement of CO(1), CO(3) and CO(4) is

similar to that of the symmetrical bridging carbonyls in $[Fe_2(CO)_9]$, since they describe three Fe(1)–CO–Fe(2) planes which form dihedral angles close to 120°. Nevertheless, in the present compound the molecular distortion result in non-bridging, semibridging and asymmetric bridging carbonyls, respectively. Finally, the Fe(1)–Fe(2) distance of 2.6116(4) Å led many authors to propose a direct metal–metal bond, although the electron count in this case is not clear.

The crystal packing shows that the molecules couple in pairs through π-stacking interactions between both rings of the bpy ligands (Fig. 7 and Table 3). The interacting rings form a tilt angle of 5.02°, with a distance between centroids of 3.62 Å and displacement angles 20.2° and 24.8°. Although some normal distances are less than 3 Å, there is no π-overlap between rings of different pairs: the nearest centroids are more than 4.70 Å apart since the displacement angles are greater than 48°. Nevertheless, we can consider that pairs are stacked along the x-axis by two weak reciprocal interdimer hydrogen interactions between H(14) of one pair and the aromatic system of the bpy ring containing N(2) of the nearest one. Weak hydrogen interactions between the carbonylic oxygen atom of CO(4) belonging to a stack and both H(16) and H(10) atoms of surrounding stacks maintain the crystal integrity.

2.3.4. $[Fe_2(CO)_7(phen)]$ (**2b**)

The structure consists of neutral dinuclear molecules (Fig. 8). Selected bond lengths and angles are given in Table 2.

The core of the molecule is similar to that depicted for compound **2a**. The geometry around Fe(1) is a less distorted octahedron whose *trans* angles range from 163.2° to 173.2° and the *cis* angles range from 80.5° to 102.8°, with a mean of 90(7)°. The Fe(2) atom is bound to the four carbon atoms C(3) to C(6), which are 0.11 Å inside their least-squares plane, which conforms the base of an SPY environment, and to C(7), which is placed in the apical position. The metal is 0.29 Å displaced from the basal plane towards the CO(7) ligand. The SPY geometry is verified by the values of the Addison's and Homes' percentages (19 and 18%, respectively). As in **2a**, the carbonyls CO(4) and CO(3) bridge the iron atoms in asymmetrical and semibridging modes, respectively, whereas CO(1) is terminal to Fe(1). The Fe(1)–Fe(2) distance is shorter, 2.5950(4) Å, although the previous observations on the metal–metal bond are also applicable to this case.

The analysis of the crystal packing shows a similar molecular arrangement to **2a**, but with an additional aromatic ring in the heterocyclic ligand, which favours a higher number of π-stacking interactions, involving all the aligned molecules (see Fig. 9 and Table 3).

The stack is formed along the z-axis, with which the interacting rings containing N(1) and N(3) form angles of 56.9° and 56.1°, respectively. Two kinds of π–π interactions were detected (Fig. 9). Between one molecule and the neighbour placed at $(-x, 1-y, 1-z)$, there is a reciprocal double contact of the rings containing N(1) and N(3) of two neighbouring molecules: they form a tilt angle of 2.3° with intercentroid distances of 3.64 Å and displacement angles of 20.6° and 22.9°. The possible overlap between rings containing N(1) of adjacent molecules has been neglected as the separation (3.91 Å) and displacement (29.8°) are limiting values. The π–π interaction of the former molecule and its $(1-x, 1-y, 1-z)$ counterpart is due to the overlap between the parallel rings containing N(3), with $D = 3.62$ Å and displacement angles of 26.1°. This overlap is rendered more efficiently by a double reciprocal hydrogen interaction between H(13) and the ring containing N(2) and weak C(14)–H(14)···O(3) hydrogen bonds. Inter-stacking interactions are established through C(18)–H(18)···O(1) bonds.

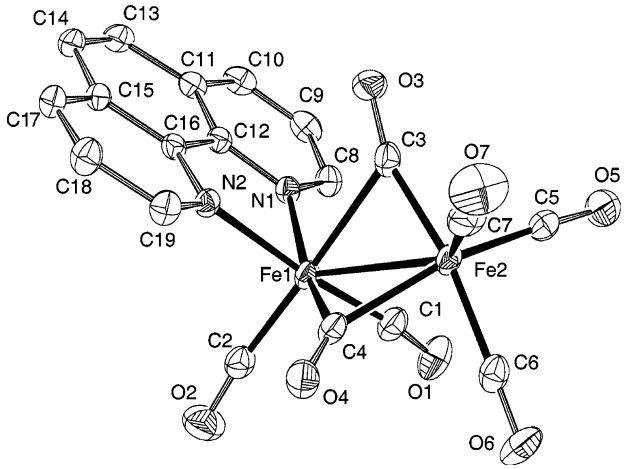

Fig. 8. ORTEP view of the molecular structure of $[Fe_2(CO)_7(phen)]$ (**2b**). Thermal ellipsoids are drawn at 50% probability level. H atoms have been omitted for clarity.

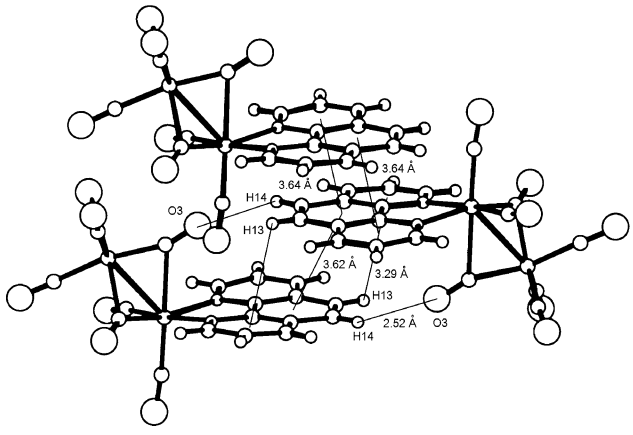

Fig. 9. π-Stacking interactions in $[Fe_2(CO)_7(phen)]$ (**2b**).

2.4. AIM analysis of the electronic density

The electronic structure of the di-iron nonacarbonyl derivatives has been widely studied because of the wide-ranging properties of their bridging carbonyl groups, and also because of the controversy surrounding the Fe–Fe bond and its consequences for the electron-counting rules [46–48]. To our knowledge, α-diimine derivatives have not been studied from this perspective, and so we performed ab initio calculations on their crystal structures.

In order to analyse and compare the bonding in **1a** and **1b** and **2a** and **2b** complexes, we applied Bader's AIM theory [31,49]. The methodology obviates the need to analyse the individual molecular orbitals of chemical systems with a large number of electrons, as it focuses on the topological analysis of the total electronic density (ρ) in the space occupied by the molecule. The electronic density is calculated from the wavefunctions obtained from standard quantum chemistry methods, and it is independent of the orbital representation chosen.

An introductory overview of how the electron density is distributed around two bonded atoms shows that near the nuclei a spherical high concentration of ρ is expected, since the core electrons do not participate in the bond. The valence density surrounds the former, and when two atoms form a chemical bond, some of the valence electron density concentrates in the interatomic region, corresponding to the positive overlap of the valence atomic orbitals. As a consequence, when we pass from one nucleus to the other along the interatomic line (more rigorously, following the bond path), the density first decreases as we leave the first core, then reaches a minimum near the centre of the line and rises again as we approach the second core: the valence electron density looks like two contacting viscous liquid drops. Nevertheless, this minimum of electronic density in two bonded atoms is only observed over the interatomic direction: if we look at the perpendicular plane, density grows when approaching the density minimum that was observed over the interatomic line. Bader's group translated this observation to a mathematical formulation: the Hessian matrix of ρ at this characteristic point shows one positive eigenvalue (a vector that coincides with the interatomic line, on which ρ decreases as we approach this point) and two negative eigenvalues (two vectors perpendicular to the anterior, where density grows towards this point). This point is symbolized by the $(3,-1)$ notation: the first digit indicates the three dimensions of real space, whereas the second is the result of adding the value $+1$ for each positive eigenvalue and -1 for each negative one. Any point that satisfies these conditions is called a bond critical point (BCP) in Bader's model and it is a necessary condition for the presence of a chemical bond. The electronic density value at a BCP is a measure of the strength of the bond.

Similarly, other types of critical points are found on ρ: (a) the $(3,-3)$ critical points, named attractors, that correspond to atomic cores: density grows when approaching them from any direction; (b) the $(3,+1)$ ring critical points (RCPs), which indicate a cyclic arrangement of bonds around them: density decreases when approaching these points across the ring plane (this is equivalent to leaving the ring bonds), but grows from the out-of-plane direction; (c) $(3,+3)$ cage critical points (CCPs) which correspond to a inner zone of the molecule where density reaches a local minimum. Topologically, the number of critical points of each type in a finite molecule must satisfy the Hopf–Poincaré condition: Attractors-BCP + RCP-CCP = 1. Further information can be obtained from the analysis of the Laplacian function of the electronic density ($\nabla^2\rho$) at the BCP: a negative value indicates that the BCP is placed in a density concentration region, whereas positive sign indicates a local depletion of the electronic density. BCPs corresponding to classical bonds have negative Laplacians, as electronic density in the bonding region has been concentrated as the result of the formation of the bond; this coincides with molecular regions where potential energy is dominant.

From the AIM analyses of $[Fe(CO)_3(bpy)]$ (**1a**) and $[Fe(CO)_3(phen)]$ (**1b**), we can extract some common trends for compounds of this kind. The parameters for electronic density at the BCPs found for the internal α-diimine bonds lie in the normal ranges described in the literature (see Table 4). Nevertheless, Fe–N, Fe–C and C–O bonds show a distinct characteristic: all of them have positive Laplacian at the BCP (see Table 5). The finding that these latter BCPs lay within density depletion regions, where kinetic electronic energy dominates, could indicate backbonding character. As expected, C≡O triple bonds have high electronic density at the BCP, but in Fe–N they almost double it, indicating an optimum bonding for these chelating ligands. Otherwise, Fe–CO BCPs have low density and are located in strongly depleted regions. The only remarkable difference found between axial and equatorial Fe–C bonds is that the Laplacian values at the axial BCPs are almost 20% more positive than for the equatorial ones, thus these *trans*-placed BCPs lie in zones where kinetic electronic energy predominates over potential.

Table 4
Ranges of values of the electronic density (e $Å^{-3}$) and its Laplacian (in parentheses, all negative values) at the BCPs of the α-diimine ligands in compounds **1a**, **1b**, **2a** and **2b**

Bond	Compounds **1a-b**, **2a-b**
C–H (−1.6 to −1.8)	0.37–0.38
C–C (aromatic)	0.30–0.33 (−0.75 to −0.94)
C–N (aromatic)	0.31–0.32 (−0.81 to −0.92)
C–C (single)	0.28 (−0.73 to −0.75)

Table 5
Ranges of values of the electronic density (e $Å^{-3}$) and its Laplacian (in parentheses, all positive values) at the BCPs of the terminal ligands in compounds **1a**, **1b**, **2a** and **2b**

Bonds	Compounds **1a** and **1b**		Compounds **2a** and **2b**		
	Fe-L (axial)	Fe-L (equat)	Fe(1)-L	Fe(2)-L (apical)	Fe(2)-L (basal)
Fe–N	0.89–0.05 (0.44–0.45)	0.87–0.89 (0.46–0.47)	0.75–0.81 (0.39–0.40)		
Fe-CO (terminal)	0.15 (0.56–0.58)	0.15 (0.66)	0.14–0.15 (0.56–0.59)	0.15 (0.56)	0.13–0.14 (0.54–0.56)
CO (terminal)	0.46 (0.36–0.43)	0.45–0.46 (0.39–0.46)	0.46–0.47 (0.41–0.50)	0.46–0.47 (0.45–0.52)	0.47–0.48 (0.50–0.56)

For the dinuclear complexes **2a** and **2b**, most of these characteristics are retained, although certain differences should be emphasized. In the metal coordination spheres (see Table 5), the Fe(1) centres have changed from TBPY-pentacoordination in mono-iron compounds to nearly octahedral in these dinuclear systems. Since the same valence density is now shared with an extra iron-ligand bond (6 in octahedra instead of 5 in TBPY), the BCP densities at the Fe–N bonds are about 10% lower. Nevertheless, the low densities at the Fe(1)–CO(terminal) bond BCPs remain unchanged, and so stability is not compromised. Concerning the SPY-pentacoordinated Fe(2) environment, the AIM analysis shows that the Fe(2) bond to apical CO(7) has its BCP parameters similar to the above-mentioned Fe(1)–CO(terminal) bonds, whereas that of basal terminal carbonyls are 10% less electron dense, and consequently weaker.

The dinuclear core region formed by the Fe(1)–C(3)–Fe(2)–C(4) ring deserves special attention. Neither the original AIM program nor its Gaussian implementation detected any BCP in the proximities of the Fe–Fe internuclear line. On the contrary, only one RCP was detected near the metal–metal internuclear line in each complex, thus representing a minimum of electronic density in the intermetallic region (see Fig. 10), the contrary to what would be expected for a di-iron bond [50]. As the necessary condition for a Fe–Fe bond is not accomplished, the AIM theory rules out metal–metal bonding in these dinuclear compounds. These results agree with former studies on the electronic density of the related $[Fe_2(CO)_9]$ system, where AIM analysis [46] detected a CCP over the intermetallic line, while electron localization function (ELF) techniques [47] exclusively localized bridging electrons over the Fe–C lines. Although MO analysis of di-iron nonacarbonyl is not straightforward, most recent papers [48] agree that any Fe–Fe interaction must be repulsive, and that the carbonyl bridges keep the cluster integrity.

The topological analysis of the bridging bonds is summarized in Table 6. The BCPs belonging to the Fe(1)–C(4) and Fe(2)–C(3) bonds, both placed in *trans* position to the Fe–N bonds, have density parameters close to that of the rest of terminal Fe–CO bonds, but less positive Laplacian values. On the other hand, Fe(2)–C(4) and, especially, Fe(1)–C(3) bonds, have low density at the BCPs, which lie in a region in which the Laplacian is close to zero. These features support the structural classification of CO(4) and CO(3) as asymmetric bridging and semibridging carbonyls, respectively. All these findings suggest that the weakest bridging bond, Fe(1)–C(3), is formed at the expense of the electronic density originally involved in terminal Fe(1)–N bonds, whereas Fe(2)–C(4) bonds correspond to a geometrically less stable rearrangement of the original Fe(2) pentacoordination through a Berry-pseudorrotation. This analysis agrees with the reaction mechanism we proposed earlier for the formation of the dinuclear complexes (Scheme 5).

This approach may also explain the formation of $[Fe_2(CO)_9]$ on exposure to UV radiation of a glacial acetic acid solution of $[Fe(CO)_5]$ [51]. In that case, the absence of the nitrogenated ligands allows the formation of three symmetric equivalent CO bridges, allowing us to visualize the dinuclear complex as two face-sharing octahedrons. As in our compounds, bridging would be exclusively due to CO molecules, with no recourse to iron–iron bonding. In fact, the cores of both structures are geometrically similar, with iron and carbon atoms placed at equivalent positions (Scheme 6).

3. Experimental

All manipulations were performed under an atmosphere of prepurified nitrogen with standard Schlenk techniques. Solvents were distilled from appropriate drying agents. Column chromatography was performed in inert atmosphere using silica 60 (35–70 μm), which had been previously degassed under vacuum at 150 °C for 48 h and kept under nitrogen. Compounds $[Fe(CO)_3(bda)]$ [39], $[Fe_2(CO)_9]$ [51], $[Fe_3(CO)_{12}]$ [52] and $[Fe_5C(CO)_{15}]$ [53] were prepared according to literature procedures. Anhydrous TMNO was obtained from Aldrich's commercial dihydrate and dehydrated by vacuum sublimation. Samples for analyses and physical measurements were prepared in a glove box.

Elemental analyses (C, H and N) were carried out at the Institut de Química Bio-Orgànica, CSIC (Barcelona). Although crystalline samples packed under N_2

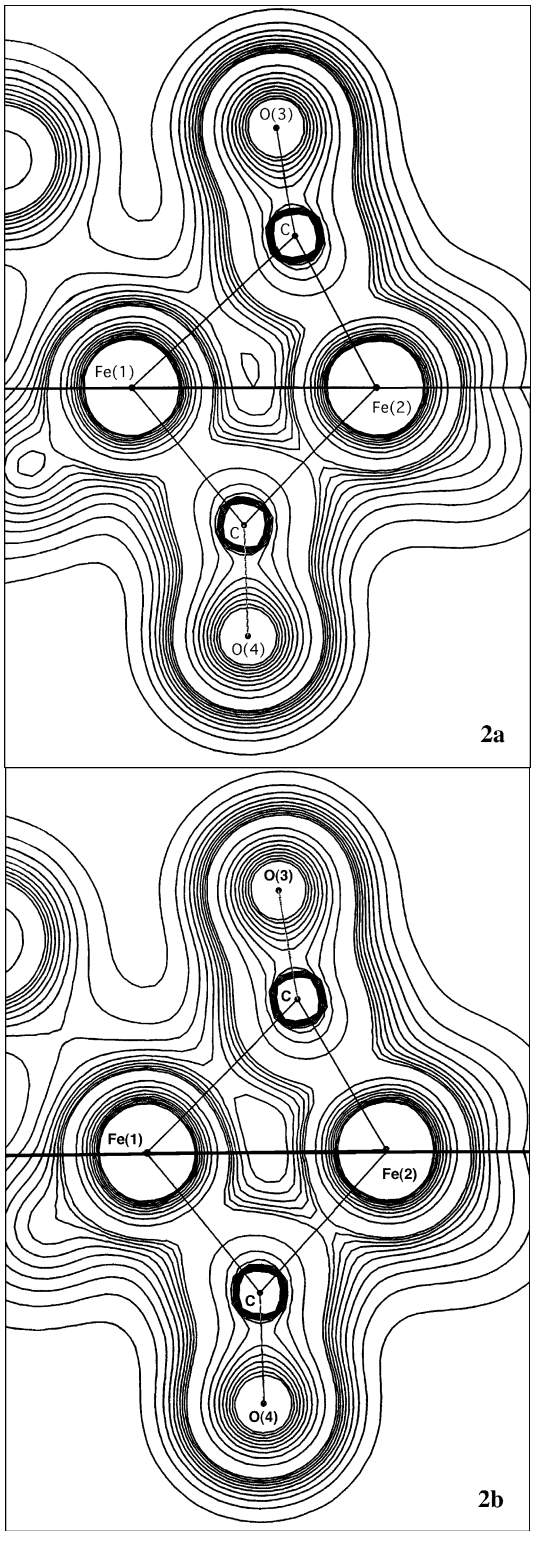

Fig. 10 (*Continued*)

Fig. 10. Contour plots for the electronic density of the core regions of compounds **2a** and **2b**. The central lines indicate the Fe(1)–Fe(2) axis. The upper sides correspond to the plots of the planes containing the Fe(1)–C(3)–Fe(2) atoms, whereas the lower ones contain atoms Fe(1)–C(4)–Fe(2) (both planes form a dihedral angle near 120°). Internal contours are plotted each 0.10 e $Å^{-3}$, and involve C–O bonds density and the outer shells of the atomic cores. External contours step 0.01 e $Å^{-3}$; they involve the Fe-L BCPs and reveal, especially in **2b**, the density hole in the intermetallic region.

Table 6
Ranges of values of the electronic density (e $Å^{-3}$) and its Laplacian (all positive values) at the BCPs of the bridging ligands in compounds **2a** and **2b**

Bond	Density	Laplacian
Fe(1)–CO(3)	0.05	0.07–0.09
CO(3)–Fe(2)	0.13–0.14	0.43–0.47
C(3)–O(3)	0.45	0.37–0.39
Fe(1)–CO(4)	0.13	0.28
CO(4)–Fe(2)	0.09	0.18
C(4)–O(4)	0.43	0.26–0.27

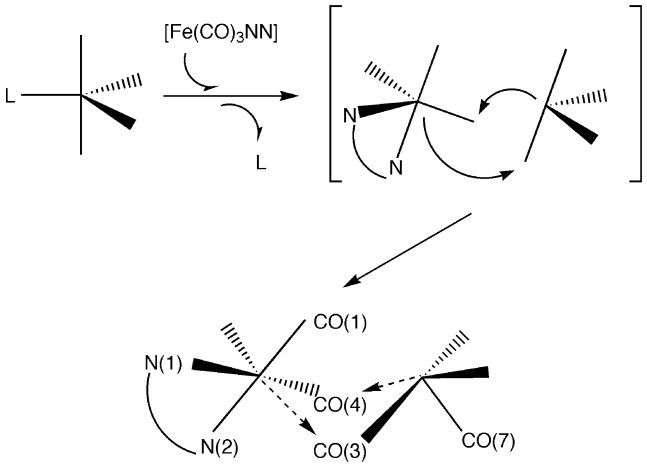

Scheme 5.

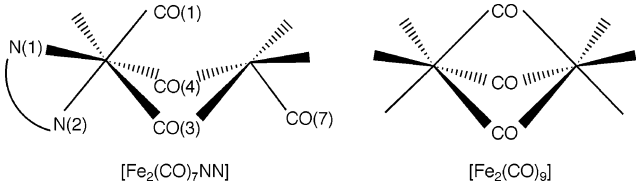

Scheme 6.

were provided, unsatisfactory results were obtained because of incomplete combustion in spite of the wide range of catalyzers assayed. Infrared spectra were recorded in THF solutions or in KBr pellets on an FT-IR 520 Nicolet spectrophotometer. ^{1}H-NMR and $^{13}C\{^{1}H\}$-NMR spectra were taken on a Bruker DRX 250 and a Varian Unity 300 spectrometers. $^{1}H–^{13}C\{^{1}H\}$ heterocorrelation NMR spectra (HSQC, HMQC and HMBC) were obtained at the Unitat de Ressonància Magnètica Nuclear of the Universitat de Barcelona on a Bruker DMX 500 spectrometer (spectral data are collected in Table 1). Mass spectrometry was carried

out at the Servei d'Espectrometria de Masses of the Universitat de Barcelona. FAB(+) and FAB(−) techniques were applied on THF solutions using a VG-QUATTRO spectrometer with NBA as a matrix. MALDI spectra were obtained on a Voyager DE-RP time-of-flight (TOF) mass spectrometer equipped with a nitrogen laser (337 nm, 3 ns pulse). Data were acquired in the linear or reflectron mode operation with delay times of 125–200 ns. Samples were prepared in a glove box using 2,5-dihydroxy-benzoic acid (DHB) as a matrix and THF or benzene as solvent. Neither technique allowed clear identification of molecular peaks of any product, as recombination occurred and peaks with *m/z* corresponding to $[Fe_3(CO)_{10}NN]$, $[Fe_2(CO)_7NN]$ and $[Fe_3(CO)_3NN]$ ions were observed for solutions of pure type **1** and **2** compounds.

3.1. General procedure for the synthesis of *1a–1d* compounds

A solution of α-diimine and $[Fe(CO)_3(bda)]$ in 25 ml of toluene was stirred, at room temperature, for several hours (4–5 h) until the 2065 cm^{-1} band in the infrared spectrum, belonging to iron tricarbonyl benzylideneacetone, disappeared. The blue solution was evaporated to dryness. The residue was then picked up in THF–hexane (25%) and chromatographed with the same solvent over 2 cm × 15 cm silica column. The blue fraction, on removal of the solvent, gave $[Fe(CO)_3$(α-diimine)].

3.1.1. $[Fe(CO)_3(bpy)]$ (*1a*)

Reagents: 567 mg (3.63 mmol) of 2,2′-bpy and 520 mg (1.82 mmol) of $[Fe(CO)_3(bda)]$. Yield: 253 mg, 47%. Selected IR data (KBr): [ν(CO)] 1968 (vs), 1897 (s), 1862 (vs).

3.1.2. $[Fe(CO)_3(phen)]$ (*1b*)

Reagents: 680 mg (3.77 mmol) of 1,10-phen and 540 mg (1.89 mmol) of $[Fe(CO)_3(bda)]$. Yield: 315 mg, 52%. Selected IR data (KBr): [ν(CO)] 1975 (s), 1904 (s), 1862 (vs).

3.1.3. $[Fe(CO)_3(4,4'\text{-}Me_2bpy)]$ (*1c*)

Reagents: 1.09 g (5.91 mmol) of 4,4′-Me_2bpy and 850 mg (2.97 mmol) of $[Fe(CO)_3(bda)]$. Yield: 520 mg, 54%. Selected IR data (KBr): [ν(CO)] 1971 (s), 1890 (vs), 1869 (vs).

3.1.4. $[Fe(CO)_3(4,7\text{-}Me_2phen)]$ (*1d*)

Reagents: 946 mg (4.54 mmol) of 4,7-Me_2phen and 650 mg (2.27 mmol) of $[Fe(CO)_3(bda)]$. Yield: 365 mg, 46%. Selected IR data (KBr): [ν(CO)] 1968 (s), 1949 (vs), 1929 (vs), 1883 (s).

3.2. General procedure for the synthesis of *2a–2d* compounds

To a precooled suspension of $[Fe_2(CO)_9]$ in 25 ml of THF at −78 °C were added a solution of the α-diimine in 10 ml of THF and a suspension of TMNO in 5 ml of THF. The mixture was stirred for several hours (3–4 h) and then filtered off and evaporated to dryness. The residue was chromatographed over 2 cm × 20 cm silica column. Elution with THF:hexane (50%) developed a blue band that, on removal of the solvent gave $[Fe(CO)_3$(α-diimine)] (**1**). Elution with THF:hexane (10%) developed a lilac fraction that, on removal of the solvent, afforded $[Fe_2(CO)_7$(α-diimine)] (**2**).

3.2.1. $[Fe_2(CO)_7(bpy)]$ (*2a*) and $[Fe(CO)_3(bpy)]$ (*1a*)

Reagents: 509 mg (1.40 mmol) of $[Fe_2(CO)_9]$, 440 mg (2.82 mmol) of 2,2′-bpy and 420 mg (5.58 mmol) of TMNO. Yield: 46 mg (16%) of $[Fe(CO)_3$(2,2′-bpy)] (**1a**) and 267 mg (57%) of $[Fe_2(CO)_7$(2,2′-bpy)] (**2a**). Selected IR data for **2a** (KBr): [ν(CO)] 2040 (s), 1982 (s, sh), 1954 (vs), 1884 (m), 1756 (m).

3.2.2. $[Fe_2(CO)_7(phen)]$ (*2b*) and $[Fe(CO)_3(phen)]$ (*1b*)

Reagents: 660 mg (1.81 mmol) of $[Fe_2(CO)_9]$, 330 mg (1.83 mmol) of 1,10-phen and 270 mg (3.59 mmol) of TMNO. Yield: 60 mg (25%) of $[Fe(CO)_3$(1,10-phen)] (**1b**) and 229 mg (62%) of $[Fe_2(CO)_7$(1,10-phen)] (**2b**). Selected IR data for **2b** (KBr): [ν(CO)] 2036 (s), 1991 (m), 1945 (vs), 1908 (w), 1853 (m), 1759 (m).

3.2.3. $[Fe_2(CO)_7(4,4'\text{-}Me_2bpy)]$ (*2c*) and $[Fe(CO)_3(4,4'\text{-}Me_2bpy)]$ (*1c*)

Reagents: 500 mg (1.37 mmol) of $[Fe_2(CO)_9]$, 253 mg (1.37 mmol) of 4,4′-Me_2bpy and 206 mg (2.74 mmol) of TMNO. Yield: 50 mg (22%) of $[Fe(CO)_3$(4,4′-Me_2bpy)] (**1c**) and 230 mg (68%) of $[Fe_2(CO)_7$(4,4′-Me_2bpy)] (**2c**). Selected IR data for **2c** (KBr): [ν(CO)] 2043 (s), 1993 (m), 1962 (vs), 1836 (m), 1756 (m).

3.2.4. $[Fe_2(CO)_7(4,7\text{-}Me_2phen)]$ (*2d*) and $[Fe(CO)_3(4,7\text{-}Me_2phen)]$ (*1d*)

Reagents: 540 mg (1.48 mmol) of $[Fe_2(CO)_9]$, 309 mg (1.48 mmol) of 4,7-Me_2phen and 223 mg (2.96 mmol) of TMNO. Yield: 38 mg (15%) of $[Fe(CO)_3$(4,7-Me_2phen)] (**1d**) and 233 mg (61%) of $[Fe_2(CO)_7$(4,7-Me_2phen)] (**2d**). Selected IR data for **2d** (KBr): [ν(CO)] 2037 (s), 1988 (s), 1967 (s), 1946 (vs), 1896 (w),1854 (m), 1748 (m).

3.3. Synthesis of compounds *1e* and *2e*

For ligand **e**, the best yield synthesis of both the mono- and di-iron derivatives was afforded departing from $[Fe_2(CO)_9]$. The procedure was the same as for **2a**–

2d derivatives. In this case, elution with THF:hexane (50%) developed a blue band that, on removal of the solvent, gave [Fe(CO)$_3$(2,9-Me$_2$phen)] (**1e**). A subsequent elution with THF:hexane (10%) developed a lilac fraction that, on removal of the solvent, afforded [Fe$_2$(CO)$_7$(2,9-Me$_2$phen)] (**2e**). Reagents: 510 mg (1.40 mmol) of [Fe$_2$(CO)$_9$], 292 mg (1.40 mmol) of 2,9-Me$_2$phen and 210 mg (2.80 mmol) of TMNO. Yield: 220 mg (90%) of [Fe(CO)$_3$(2,9-Me$_2$phen)] (**1e**) and 27 mg (7%) of [Fe$_2$(CO)$_7$(2,9-Me$_2$phen)] (**2e**). Selected IR data for **1e** (KBr): [ν(CO)] 1968 (s), 1883 (m), 1855 (vs). Selected IR data for **2e** (KBr): [ν(CO)] 2073 (m), 2007 (vs), 1961 (vs), 1939 (s), 1911 (s).

3.4. General procedure for single-crystal structural determination of compounds *1a* and *2b*, and *2a* and *2b*

Crystals suitable for X-ray diffraction of **1a**·0.5C$_{10}$H$_8$N$_2$, **1b**, **2a** and **2b** were obtained from THF solutions layered with *n*-hexane at ca. 4 °C. The crystal data and experimental details were summarized in Table 7. Diffraction data were collected on a Bruker SMART CCD 1K area-detector single-crystal diffractometer using a Mo–K$_\alpha$ ($\lambda = 0.71073$ Å) X-ray source and a graphite monochromator. A total of 1271 frames of data were collected using the phi-omega scan method. The first 50 frames were collected at the end of data collection to monitor for decay. The crystals used for the diffraction study showed no decomposition during data collection. Absorption corrections were applied using the SADABS program [54]. The structures were solved by direct methods using the SHELXS-97 computer program [55] for crystal structure determination and by full-matrix least-squares method of F^2, with the SHELXL-97 computer program [56]. Hydrogen atoms were included in calculated positions and refined in riding model. The weighing schemes employed were of the form $w = [\sigma^2 F_o^2 + (AP)^2 + BP]$ and $P = (|F_o|^2 + 2|F_c|^2)/3$, with $A = 0.0358$ and $B = 0.4487$ for **1a**, $A = 0.0455$ and $B = 0.1845$ for **1b**, $A = 0.0441$ and $B = 0.1906$ for **2a**, and with $A = 0.0464$ and $B = 0.0000$ for **2b**.

3.5. Computational details

The wavefunction sets of the compounds were obtained from density functional theory [57] calculations carried out by the Gaussian 98 package [58] running on an IBM RS/6000 3AT workstation. The Becke three-parameter exchange function [59] (B3) in conjunction with the Lee–Yang–Parr [60] (LYP) correlation functional was employed, as this method is believed to be considerably accurate and efficient. The basis set for the iron centres was 6-3111+G whereas for the rest of the atoms was 6-311G*. Calculations were single-point ones

Table 7
Crystal data and structure refinement details for complexes **1a**·0.5C$_{10}$H$_8$N$_2$, **1b**, **2a** and **2b**

	1a·0.5C$_{10}$H$_8$N$_2$	**1b**	**2a**	**2b**
Color, habit	brown, block	brown, block	purple, plate	purple, block
Max. crystal dimensions (mm^3)	0.55 × 0.40 × 0.20	0.20 × 0.20 × 0.15	0.25 × 0.20 × 0.05	0.35 × 0.30 × 0.25
Chemical formula	C$_{18}$H$_{12}$FeN$_3$O$_3$·0.5C$_{10}$H$_8$N$_2$	C$_{15}$H$_8$FeN$_2$O$_3$	C$_{17}$H$_8$Fe$_2$N$_2$O$_7$	C$_{19}$H$_8$Fe$_2$N$_2$O$_7$
Formula weight	374.16	320.09	463.95	487.97
Crystal system	monoclinic	monoclinic	triclinic	monoclinic
Space group	$P2_1/n$ (No. 14)	$P2_1/c$ (No. 14)	$P\bar{1}$ (No. 2)	$P2_1/c$ (No. 14)
a (Å)	7.2180(1)	10.5337(3)	6.9559(4)	7.9496(1)
b (Å)	14.1335(3)	7.4265(2)	10.3965(6)	17.0560(1)
c (Å)	15.8197(3)	17.5315(1)	12.3717(7)	13.8789(2)
α (°)	90.0	90.0	78.570(1)	90.0
β (°)	101.936(1)	104.853(2)	84.363(1)	101.647(1)
γ (°)	90.0	90.0	82.442(1)	90.0
V (Å^3)	1578.96(5)	1324.38(5)	866.92(9)	1843.07(4)
Z	4	4	2	4
D_{calc} (g cm^{-3})	1.574	1.605	1.777	1.759
T (K)	173(2)	173(2)	173(2)	173(2)
Scan width (°)	1.95–28.23	2.00–28.28	1.68–28.29	1.92–28.36
μ(Mo–K$_\alpha$) (mm^{-1})	0.978	1.149	1.718	1.621
Transmission factors	0.6153–0.8284	0.8465–0.8028	0.9190–0.6733	1.0000–0.8040
No. of reflections collected	10749	8886	6090	12513
No. of reflections unique (R_{int})	3889 (0.0308)	3238 (0.0381)	4181 (0.0148)	4537 (0.0356)
No. of reflections observed	3170	2495	3622	3703
Goodness-of-fit (on F^2)	1.025	1.028	1.033	1.015
R_1, wR_2 [$I > 2\sigma(I)$]	0.0311, 0.0725	0.0365, 0.0834	0.0284, 0.0733	0.0309, 0.0764
All data	0.0448, 0.0783	0.0574, 0.0925	0.0352, 0.0766	0.0441, 0.0830

$R_1 = \Sigma|F_o - F_c|/\Sigma|F_o|$, $wR_2 = \Sigma(F_o^2\text{-}F_c^2)^2/\Sigma w(F_o^2)^{1/2}$.

run over the crystallographic geometry without further optimization.

Wavefunction files were treated with the AIMPAC [61] suite of programs, modified to account for the input size. Electronic density and Laplacian values were analysed using the standard built-in parameters. Graphical analysis and representations were performed by means of the MOLDEN [62] software.

4. Supplementary material

Crystallographic data for structural analysis have been deposited at the Cambridge Crystallographic Data Centre, with CCDC Nos. 201409, 201410, 201411 and 201412 for compounds $[Fe(CO)_3(bpy)]\cdot 0.5C_{10}H_8N_2$, $[Fe(CO)_3(phen)]$, $[Fe_2(CO)_7(bpy)]$ and $[Fe_2(CO)_7(phen)]$, respectively. Data for the complex salt $[Fe(bpy)_3][(\mu\text{-}H)Fe_4C(CO)_{12}]_2$ has also been deposited at CCDC with No. 203409. Copies of these data may be obtained free of charge from The Director, CCDC, 12 Union Road, Cambridge CB2 1EZ, UK (Fax: +44-1223-336033; e-mail: deposit@ccdc.cam.ac.uk or www: http://www.ccdc.cam.ac.uk.).

Acknowledgements

Financial support for this work was generously given by DGICYT through grants BQU-2000-0791 (R.C.), BQU-2000-0644 (R.R.) and the CIRIT Projects 2000SGR00022 (R.C.), 1999SGR00045 (R.R.). M.D.V. was partially funded by a scholarship from the Universitat de Barcelona.

References

[1] G. VanKoten, K. Vrieze, Adv. Organomet. Chem. 21 (1982) 151.
[2] (a) T. Venalainen, J. Pursiainen, T.A. Pakkanen, J. Chem. Soc. Commun. (1985) 1348;
(b) M.I. Bruce, M.G. Humphrey, M.R. Snow, E.R.T. Tiekink, R.C. Wallis, J. Organomet. Chem. 314 (1986) 311.
[3] J. Nijhoff, M.J. Bakker, F. Hartl, G. Freeman, S.L. Ingham, B.F.G. Johnson, J. Chem. Soc. Dalton Trans. (1998) 2625.
[4] G. Freeman, S.L. Ingham, B.F.G. Johnson, M. McPartlin, I.J. Scowen, J. Chem. Soc. Dalton Trans. (1997) 2705.
[5] (a) See for example: (a) N.E. Leadbeater, J. Lewis, P.R. Raithby, G.N. Ward, J. Chem. Soc. Dalton Trans. (1997) 2511;
(b) Y. Choi, W. Wong, J. Organomet. Chem. 573 (1999) 189.
[6] W. Heiber, H. Beutner, Angew. Chem. 74 (1962) 154.
[7] P.E. Baikie, O.S. Mills, J. Chem. Soc. Commun. (1966) 707.
[8] R.J. Doedens, J. Chem. Soc. Commun. (1968) 1271.
[9] F.A. Cotton, J.M. Troup, J. Am. Chem. Soc. 96 (1974) 3438.
[10] F.A. Cotton, J.M. Troup, J. Am. Chem. Soc. 96 (1974) 1233.
[11] L.E. MacCandlish, B.D. Santarsiero, N.J. Rose, E.C. Lingafelter, Acta Crystallogr., Sect. B 35 (1979) 3053.
[12] H.W. Frühauf, G. Wolmershauser, Chem. Ber. 115 (1982) 1070.
[13] M.W. Kokkes, D.J. Stufkens, A. Oskam, J. Chem. Soc. Dalton Trans. (1983) 439.
[14] V.L. Goedken, S.M. Peng, J. Am. Chem. Soc. 96 (1974) 7826.
[15] W. Imhof, A. Gobel, R. Beckert, T. Billert, H. Gorls, J. Organomet. Chem. 590 (1999) 104.
[16] J. Breuer, H.W. Frühauf, W.J.J. Smeets, A.L. Spek, Inorg. Chim. Acta 291 (1999) 438.
[17] H.W. Frühauf, A. Landers, R. Goddard, C. Kruger, Angew. Chem. Int. Ed. Engl. 17 (1978) 64.
[18] F. Muller, I.M. Han, G. van Koten, K. Vrieze, D. Heijdenrijk, R.L. De Jong, M.C. Zoutberg, Inorg. Chim. Acta 158 (1989) 81.
[19] F. Muller, G. Van Koten, K. Vrieze, D. Heijdenrijk, Inorg. Chim. Acta 158 (1989) 69.
[20] P.P.M. de Lange, M.J.A. Kraakman, M. van Winjkoop, H.W. Frühauf, K. Vrieze, W.J.J. Smeets, A.L. Spek, Inorg. Chim. Acta 196 (1992) 151.
[21] F. Muller, G. van Koten, K. Vrieze, K.A.A. Duineveld, D. Heijdenrijk, A.N.S. Mak, C.H. Stam, Organometallics 8 (1989) 1324.
[22] D.G.A. Harshani de Silva, D.B. Leznoff, G. Impey, I. Vernik, Z. Jin, D.V. Stynes, Inorg. Chem. 34 (1995) 4015.
[23] (a) A.L. Spek, N. Veldman, N. Feiken, K. Vrieze, Private Communication to CCDC. Refcode UCIWOS;
(b) F. Muller, I.M. Han, G. Van Koten, K. Vrieze, D. Heijdenrijk, J. Van Mechelen, C.H. Stam, Inorg. Chim. Acta 158 (1989) 99.
[24] H.K. van Dijk, D.J. Stufkens, A. Oskam, M. Rotteveel, D. Heijdenrijk, Organometallics 6 (1987) 1665.
[25] M.A. de Paoli, H.W. Frühauf, F.W. Grevels, E.A. Koerner von Gustorf, W.W. Riemer, C. Kruger, J. Organomet. Chem. 136 (1977) 219.
[26] K. Fujita, K. Ito, T. Kondo, T. Mitsudo, J. Organomet. Chem. 533 (1997) 161.
[27] W. Liau, C. Chen, C. Lee, G. Lin, C. Ching, G. Lee, S. Peng, J. Chem. Soc. Dalton Trans. (1998) 353.
[28] F. Calderazzo, S. Falaschi, F. Marchetti, G. Pampaloni, J. Organomet. Chem. 662 (2002) 137.
[29] H.W. Frühauf, J. Chem. Res. (S) (1983) 216.
[30] H.W. Frühauf, J. Chem. Res. (M) (1983) 2023.
[31] R.F.W. Bader, Atoms in Molecules—A Quantum Theory, Oxford University Press, London, 1990.
[32] H.W. Frühauf, J. Chem. Res. (M) (1983) 2035.
[33] M.I. Bruce, T.W. Hamphley, B.K. Nicholson, J. Chem. Soc. Dalton Trans. (1983) 2385.
[34] M.W. Kokkes, D.J. Stufkens, A. Oskam, J. Chem. Soc. Dalton Trans. (1984) 1005.
[35] M.N. Ackermann, J.W. Naylor, E.J. Smith, G.A. Mines, N.S. Amin, M.L. Kerns, Organometallics 11 (1992) 1919.
[36] E.M. Holt, K.H. Withmire, D.F. Shriver, J. Organomet. Chem. 213 (1981) 125.
[37] J.A.S. Howell, B.F.G. Johnson, P.L. Josti, J. Lewis, J. Organomet. Chem. 39 (1972) 329.
[38] M. Brookhart, G.O. Nelson, J. Organomet. Chem. 164 (1979) 193.
[39] Q.Z. Shi, T.G. Richmond, W.C. Trogler, F. Basolo, Organometallics 11 (1982) 1033.
[40] (a) T. Tada, J. Sci. Hiroshima Univ. A 46 (1982) 73;
(b) M.E. Garcia, M.A. Juri, P.Y. Aymonino, O.E. Piro, H.A. Negri, E.E. Castellano, Inorg. Chem. 23 (1984) 948;
(c) P.C. Healy, B.W. Skelton, A.H. White, Aust. J. Chem. 36 (1983) 2057;
(d) H. Weiss, J. Strahle, Z. Naturforsch. Teil. B 39 (1984) 1453;
(e) S. Bernes, F. Secheresse, Y. Jeannin, Inorg. Chim. Acta 194 (1992) 105;
(f) S. Decurtins, H.W. Schmalle, P. Schneuwly, J. Ensling, P. Gutlich, J. Am. Chem. Soc. 116 (1994) 9521;
(g) H. Li KamWah, M. Postel, F. Tomi, L. Mordent, D. Ballivet-Tkatchenko, F. Dahan, F. Urso, New. J. Chem. 15 (1991) 629;

(h) C. Jinhua, K. Beisheng, Z. Botao, Chin. J. Onorg. Chem. 7 (1991) 301;
(i) S. Dick, Z. Kristallogr. 213 (1998) 356;
(j) H.W. Schmalle, R. Pellaux, S. Decurtins, Z. Kristallogr. 211 (1996) 533;
(k) S. Decurtins, H.W. Schmalle, P. Schneuwly, H.R. Oswald, Inorg. Chem. 32 (1993) 1888.

[41] R.R. Homes, Prog. Inorg. Chem. 32 (1984) 119 (In order to facilitate the comparison between Homes' and Addison's distortion parameters, we have reverted the former as their complementary to unity, in such a way that both equal 0 for an ideal SPY and 1 for ideal TBPY).

[42] A.W. Addison, T.N. Rao, J. Reedijk, J. Van Rijn, G.C. Verschoor, J. Chem. Soc. Dalton Trans. (1984) 2349.

[43] (a) E. Espinosa, E. Molins, C. Lecomte, Chem. Phys. Lett. 285 (1998) 170;
(b) E. Espinosa, C. Lecomte, E. Molins, Chem. Phys. Lett. 300 (1999) 745;
(c) E. Espinosa, I. Alkorta, I. Rozas, J. Elguero, E. Molins, Chem. Phys. Lett. 336 (2001) 457;
(d) E. Espinosa, E. Molins, J. Chem. Phys. 113 (2000) 5686.

[44] R. Colton, M.J. McCormick, Coord. Chem. Rev. 31 (1980) 1.

[45] F.A. Cotton, J.M. Troup, J. Am. Chem. Soc. 96 (1974) 5070.

[46] C. Bo, J.P. Sarasa, J.M. Poblet, J. Phys. Chem. 97 (1993) 6362.

[47] M. Kraupp, Chem. Ber. 129 (1996) 527.

[48] (a) R.H. Summerville, R. Hoffmann, J. Am. Chem. Soc. 101 (1979) 3821;
(b) C.W. Bauschlicher, J. Chem. Phys. 84 (1986) 872;
(c) C. Mealli, D.M. Proserpio, J. Organomet. Chem. 386 (1990) 203;
(d) A. Rosa, E.J. Baerends, New J. Chem. 15 (1991) 815;
(e) J. Reinhold, E. Hunstock, C. Mealli, New J. Chem. 18 (1994) 465;
(f) J.H. Jang, J.G. Lee, H. Lee, Y. Xie, H.F. Schaeffer, J. Phys. Chem. A 102 (1998) 5298;
(g) R. Salzmann, M. Kraupp, M.T. McMahon, E.J. Oldfield, J. Am. Chem. Soc. 120 (1998) 4771;
(h) E. Hunstock, C. Mealli, M.J. Calahorda, J. Reinhold, Inorg. Chem. 38 (1999) 5053.

[49] (a) R.F.W. Bader, S. Johnson, T.H. Tang, P.L.A. Popelier, J. Phys. Chem. 100 (1996) 15398;
(b) R.F.W. Bader, Coord. Chem. Rev. 197 (2000) 71.

[50] Nevertheless, the analysis technique is enough sensitive to detect the intramolecular hydrogen interactions C(17)–H(17)···O(4) in **2a** and C(19)–H(19)···O(4) in **2b**, with densities at the BCPs smaller than 0.01 e $Å^{-3}$.

[51] E.H. Braye, W. Hübel, Inorg. Synth. 8 (1966) 178.

[52] W. McFarlane, G. Wilkinson, Inorg. Synth. 8 (1966) 181.

[53] M. Tachikawa, R.L. Geerts, E.L. Mutterties, J. Organomet. Chem. 213 (1981) 11.

[54] G.M. Sheldrick, SADABS program: a program for empirical absorption correction of area detector data, University of Göttingen, Germany, 1996.

[55] G.M. Sheldrick, SHELXS-97, a program for crystal structure determination, University of Göttingen, Germany, 1997.

[56] G.M. Sheldrick, SHELXS-97, a computer program, a program for crystal structure refinement, University of Göttingen, Germany, 1997.

[57] W. Kohn, L.J. Sham, Phys. Rev. 140 (1965) A1133.

[58] M.J. Frisch, G.W. Trucks, H.B. Schlegel, G.E. Scuseria, M.A. Robb, J.R. Cheeseman, V.G. Zakrzewski, J.A. Montgomery, Jr., R.E. Stratmann, J.C. Burant, S. Dapprich, J.M. Millam, A.D. Daniels, K.N. Kudin, M.C. Strain, O. Farkas, J. Tomasi, V. Barone, M. Cossi, R. Cammi, B. Mennucci, C. Pomelli, C. Adamo, S. Clifford, J. Ochterski, G.A. Petersson, P.Y. Ayala, Q. Cui, K. Morokuma, D.K. Malick, A.D. Rabuck, K. Raghavachari, J.B. Foresman, J. Cioslowski, J.V. Ortiz, A.G. Baboul, B.B. Stefanov, G. Liu, A. Liashenko, P. Piskorz, I. Komaromi, R. Gomperts, R.L. Martin, D.J. Fox, T. Keith, M.A. Al-Laham, C.Y. Peng, A. Nanayakkara, C. Gonzalez, M. Challacombe, P.M.W. Gill, B. Johnson, W. Chen, M.W. Wong, J.L. Andres, C. Gonzalez, M. Head-Gordon, E.S. Replogle, J.A. Pople, Gaussian 98, Revision A.7, Gaussian, Inc, Pittsburgh PA, 1998.

[59] A.D. Becke, J. Chem. Phys. 98 (1993) 5648.

[60] C. Lee, W. Yang, R.G. Parr, Phys. Rev. B 37 (1982) 785.

[61] F.W. Biegler-Konig, R.F.W. Bader, T. Tang, J. Comput. Chem. 3 (1982) 317.

[62] G. Schaftenaar, MOLDEN, a package for displaying molecular density, CMB1, University of Nijmegen, The Netherlands, 1991.